

# Probing $HZ\gamma$ and $H\gamma\gamma$ anomalous couplings in the process $e^+e^- \rightarrow H\gamma^*$

CAO Qing-Hong(曹庆宏)<sup>1,2,3;1)</sup> WANG Hao-Ran(王浩然)<sup>1;2)</sup> ZHANG Ya(张亚)<sup>1;3)</sup>

<sup>1</sup> Department of Physics and State Key Laboratory of Nuclear Physics and Technology, Peking University, Beijing 100871, China

<sup>2</sup> Collaborative Innovation Center of Quantum Matter, Beijing 100871, China

<sup>3</sup> Center for High Energy Physics, Peking University, Beijing 100871, China

**Abstract:** We propose to measure the  $HZ\gamma$  and  $H\gamma\gamma$  anomalous couplings in the process  $e^+e^- \rightarrow H\gamma$  with the sequential decay of  $H \rightarrow b\bar{b}$ . The discovery potential of observing the anomalous couplings are explored in detail. Our study shows that future electron-positron colliders have great potential to test the  $HZ\gamma$  and  $H\gamma\gamma$  couplings. Conservative bounds on the two anomalous couplings are also derived when no new physics signal is detected on top of the SM backgrounds.

**Key words:** Higgs physics, rare decay, electron-positron collision

**PACS:** 13.66.FG, 13.66.Jn **DOI:** 10.1088/1674-1137/39/11/113102

## 1 Introduction

After the discovery of the Higgs boson, precision measurement of its properties has been placed on the agenda, especially the measurement of its rare decay modes as the Standard Model (SM) contribution is fairly small. Observing a deviation from the SM prediction would shed light on new physics (NP) beyond the SM. Among the rare decay modes of the Higgs boson, the  $\gamma\gamma$  mode is bounded much more tightly than the others. Its best-fit signal strength relative to the SM prediction is  $1.17 \pm 0.27$ , obtained by the ATLAS collaboration [1], and  $1.14^{+0.26}_{-0.23}$  from the CMS collaboration [2]. The  $H \rightarrow Z\gamma$  decay, however, is loosely constrained. The ATLAS collaboration reported an upper limit of 11 times the SM expectation at the 95% confidence level [3]. A similar result was obtained by the CMS collaboration [4], which sets an upper limit of 9.5 times the SM expectation at the 95% confidence level. Note that the  $H\gamma\gamma$  and  $HZ\gamma$  couplings are sensitive to different kinds of NP and therefore are in principle independent. Ref. [5] pointed out that the  $HZ\gamma$  coupling could be sizeably modified in certain composite Higgs models while still keeping the  $H\gamma\gamma$  coupling untouched. On the other hand, the  $HZ\gamma$  and  $H\gamma\gamma$  couplings are highly correlated in the NMSSM or MSSM-like models [6, 7]. Thus the NP models can be tested and discriminated by their different expected corrections

to the  $HZ\gamma$  and  $H\gamma\gamma$  couplings. In this work, we explore the potential of probing the anomalous couplings of  $HZ\gamma$  and  $H\gamma\gamma$  through  $H\gamma$  production at a future electron-positron collider.

The potential of probing the  $HZ\gamma$  and  $H\gamma\gamma$  couplings has been studied at  $e^+e^-$  and  $e^-e^-$  colliders through the channels of  $e^+e^- \rightarrow ZH$ ,  $e^+e^- \rightarrow e^+e^-H$ ,  $e^\pm\gamma \rightarrow He^\pm$  and  $e^+e^- \rightarrow \gamma H$  [8–16]. For the process  $e^+e^- \rightarrow H\gamma$ , the analytical expressions of its cross section have been given in Refs. [17–19]. It has also been studied in the Inert Higgs Doublet Model [6] and the MSSM [20]. Searching for the Higgs boson in the collider signature of  $e^+e^- \gamma$  at the Large Hadron Collider (LHC) is also studied in Ref. [7, 21].

In this work we assume the NP resonances are too heavy to be observed directly at the LHC, but they might generate sizable quantum corrections. Such effects are then described by an effective Lagrangian of the form

$$\mathcal{L}_{\text{eff}} = \mathcal{L}_{\text{SM}} + \frac{1}{\Lambda_{\text{NP}}^2} \sum_i (c_i \mathcal{O}_i + \text{h.c.}) + \mathcal{O}\left(\frac{1}{\Lambda_{\text{NP}}^3}\right), \quad (1)$$

where the  $c_i$ 's are coefficients that parameterize the non-standard interactions. Note that dimension-5 operators involve fermion number violation and are assumed to be associated with a very high energy scale and not relevant to the processes studied here. The relevant CP-conserving operators  $\mathcal{O}_i$  contributing to the anomalous

Received 5 May 2015

\* Supported by National Science Foundation of China (11275009)

1) E-mail: qinghongcao@pku.edu.cn

2) E-mail: haoranw@pku.edu.cn

3) E-mail: zhangya1221@pku.edu.cn



Content from this work may be used under the terms of the Creative Commons Attribution 3.0 licence. Any further distribution of this work must maintain attribution to the author(s) and the title of the work, journal citation and DOI. Article funded by SCOAP<sup>3</sup> and published under licence by Chinese Physical Society and the Institute of High Energy Physics of the Chinese Academy of Sciences and the Institute of Modern Physics of the Chinese Academy of Sciences and IOP Publishing Ltd

HZ $\gamma$  and H $\gamma\gamma$  couplings are [22]

$$\mathcal{O}_{BW} = (\phi^\dagger \tau^I \phi) B_{\mu\nu} W^{I\mu\nu}, \quad (2)$$

$$\mathcal{O}_{WW} = (\phi^\dagger \phi) W_{\mu\nu}^I W^{I\mu\nu}, \quad (3)$$

$$\mathcal{O}_{BB} = (\phi^\dagger \phi) B_{\mu\nu} B^{\mu\nu}, \quad (4)$$

$$\mathcal{O}_{\phi\phi} = (D_\mu \phi)^\dagger \phi \phi^\dagger (D_\mu \phi), \quad (5)$$

in which  $\phi^T = (0, (v+H)/\sqrt{2})$  is the Higgs doublet in the unitary gauge with  $v = 246$  GeV the vacuum expectation value,  $B_{\mu\nu} = \partial_\mu B_\nu - \partial_\nu B_\mu$  and  $W_{\mu\nu}^I = \partial_\mu W_\nu^I - \partial_\nu W_\mu^I - gf_{IJK} W_\mu^J W_\nu^K$  are the strength tensors of the gauge fields, and the Lie communicators  $[T_a, T_b] = if_{abc} T_c$  define the structure constants  $f_{abc}$ .

The  $\mathcal{O}_{\phi\phi}$  and  $\mathcal{O}_{BW}$  are constrained strongly by the electroweak precision measurements [12, 23] and are ignored in our study. On the other hand, the electroweak precision constraints on  $\mathcal{O}_{BB}$  and  $\mathcal{O}_{WW}$  are weak:  $-2.65 \leq c_{WW} \leq 2.65$  and  $-2.95 \leq c_{BB} \leq 2.95$  [24]. After spontaneous symmetry breaking, the operators yield the effective Lagrangian in terms of the mass eigenstates of photon and Z-boson as follows:

$$\mathcal{L} = \frac{v}{\Lambda^2} \left( \mathcal{F}_{Z\gamma} H Z_{\mu\nu} A^{\mu\nu} + \mathcal{F}_{ZZ} H Z_{\mu\nu} Z^{\mu\nu} + \mathcal{F}_{\gamma\gamma} H A_{\mu\nu} A^{\mu\nu} \right) \quad (6)$$

where

$$\mathcal{F}_{ZZ} = c_{WW} \cos^2 \theta_W + c_{BB} \sin^2 \theta_W,$$

$$\mathcal{F}_{\gamma\gamma} = c_{WW} \sin^2 \theta_W + c_{BB} \cos^2 \theta_W,$$

$$\mathcal{F}_{Z\gamma} = (c_{WW} - c_{BB}) \sin(2\theta_W). \quad (7)$$

Therefore, the other two couplings would exhibit a non-trivial relation which could be verified in future experiments. For example, a strong correlation between  $\mathcal{F}_{Z\gamma}$  and  $\mathcal{F}_{\gamma\gamma}$  would be generated if  $\mathcal{F}_{ZZ} \sim 0$ . The HZZ coupling is expected to be measured with an accuracy of 0.1% at the Circular Electron Positron Collider (CEPC) [25] and International Linear Collider [26]. If no deviation were observed, then  $\mathcal{F}_{ZZ} \simeq 0$ . In that case  $\mathcal{F}_{Z\gamma}$  and  $\mathcal{F}_{\gamma\gamma}$  are correlated linearly, i.e.  $\mathcal{F}_{Z\gamma} = -\tan 2\theta_W \mathcal{F}_{\gamma\gamma}$ , which could be tested at the  $e^+e^-$  collider.

## 2 H $\gamma$ production at an $e^-e^+$ collider

Now we are ready to calculate the H $\gamma$  production with the contributions of the HZ $\gamma$  and H $\gamma\gamma$  anomalous couplings. There is a subtlety in the calculation. The scattering process  $e^+e^- \rightarrow H\gamma$  is absent at tree-level in the SM when ignoring the electron mass, but it can be generated through electroweak corrections at the loop-level [17–19]. The effects of the HZ $\gamma$  and H $\gamma\gamma$  anomalous couplings, as suppressed by the NP scale  $\Lambda$ , may be comparable to those SM loop effects. Therefore, one has to consider the SM contributions as well in the discussion of NP effects in H $\gamma$  production. Here the NP effects are

assumed to be at the same order of the SM contribution to the HZ $\gamma$  and H $\gamma\gamma$  couplings. For example, an additional  $W'$  or charged Higgs boson could generate sizeable anomalous HZ $\gamma$  and H $\gamma\gamma$  couplings [27, 28]. If the NP occurs only at loop level, its contribution to the HZ $\gamma$  and H $\gamma\gamma$  coupling would be at the two loop level and therefore highly suppressed by the loop factor of  $1/16\pi^2$ .

The loop corrections in the SM can be categorized as follows: (1) the bubble diagrams originating from the external  $\gamma$  wave-function renormalization; (2) the triangle diagrams with the HZ $\gamma$ , H $\gamma\gamma$  or the Hee in the external lines; (3) the box diagrams with  $e^+e^-H\gamma$  in the external line. Figure 1 displays the representative Feynman diagrams, which also includes the HZ $\gamma$  anomalous coupling.

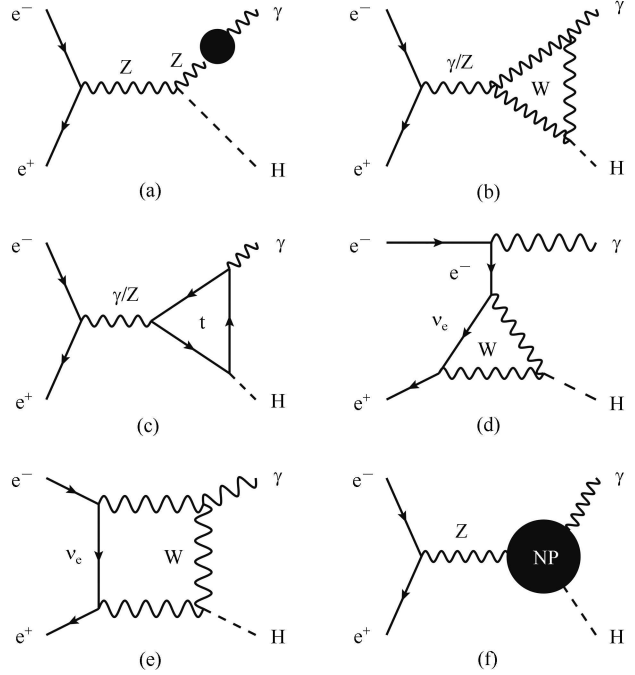


Fig. 1. Representative Feynman diagrams of the process  $e^+e^- \rightarrow H\gamma$  for the SM (a–e) and the HZ $\gamma$  anomalous coupling (f).

Consider the case of unpolarized incoming beams and ignore the electron mass. Summing over the polarization of the photon, the differential cross section of the scattering of  $e^-e^+ \rightarrow H\gamma$  can be written as [19]

$$\frac{d\sigma(e^+e^- \rightarrow H\gamma)}{d\cos\theta} = \frac{s - M_H^2}{64\pi s} \left[ u^2 (|a_1^+|^2 + |a_1^-|^2) + t^2 (|a_2^+|^2 + |a_2^-|^2) \right], \quad (8)$$

where  $\sqrt{s}$  is the energy of center-of-mass (c.m.) and the Mandelstam variables are

$$t = (p_{e^+} - p_\gamma)^2 = -(s - M_H^2)(1 - \cos\theta)/2,$$

$$u = (p_{e^-} - p_\gamma)^2 = -(s - M_H^2)(1 + \cos\theta)/2$$

with  $p_i$  the momentum of particle  $i$  and  $\theta$  the scattering angle of the photon.

The coefficient  $a_i$ , which sums contributions from all the loop diagrams and the anomalous HZ $\gamma$  and H $\gamma\gamma$  couplings, is

$$a_i^{\pm} = a_i^{\gamma\pm} + a_i^{Z\pm} + a_i^{e\pm} + a_i^{\text{box}\pm}, \quad (9)$$

where  $a_i^{\gamma}$  and  $a_i^Z$  denote the contributions of the photon and Z pole vertex diagrams,  $a_i^e$  the  $t$ -channel  $H^0 e e$  vertex corrections and  $a_i^{\text{box}}$  the contribution of the box diagrams; see Fig. 1. Detailed expression of all the coefficients in the SM can be found in Ref. [19]. The anomalous  $\mathcal{F}_{Z\gamma}$  and  $\mathcal{F}_{\gamma\gamma}$  couplings contribute only to  $a_i^{Z\pm}$  and  $a_i^{\gamma\pm}$  as follows:

$$a_1^{Z\pm} = a_2^{Z\pm} = \frac{ex^{\pm}}{4s_W c_W} \frac{1}{s - M_Z^2} \left( \frac{1}{16\pi^2} a_{\text{SM}}^{Z\pm} + \frac{2v}{\Lambda^2} \mathcal{F}_{Z\gamma} \right)$$

$$a_1^{\gamma\pm} = a_2^{\gamma\pm} = -\frac{e}{2s} \frac{1}{s} \left( \frac{1}{16\pi^2} a_{\text{SM}}^{\gamma\pm} + \frac{2v}{\Lambda^2} \mathcal{F}_{\gamma\gamma} \right)$$

where  $e$  is the electric charge,  $x^+ = -1 + 2s_W^2$ ,  $x^- = 2s_W^2$  and

$$a_{\text{SM}}^{Z\pm} = \frac{e^3 M_W}{c_W s_W^2} \left[ F_{Z,W} + \frac{m_t^2}{M_W^2} \left( \frac{1}{2} - 2s_W^2 \right) F_t \right] \quad (10)$$

$$a_{\text{SM}}^{\gamma\pm} = \frac{e^3 M_W}{s_W} \left[ F_{\gamma,W} - \frac{16m_t^2}{3M_W^2} F_t \right]. \quad (11)$$

The  $F_{Z,W}$ ,  $F_{\gamma,W}$  and  $F_t$  are obtained from the gauge boson (W and Z) and top-quark loops respectively. Only the top-quark loop is taken into account in this work as the contributions from other fermion loops are highly suppressed. The  $F_{Z,W}$ ,  $F_{\gamma,W}$  and  $F_t$  are

$$\begin{aligned} F_{Z,W} &= 2 \left[ \frac{M_H^2}{M_W^2} (1 - 2c_W^2) + 2(1 - 6c_W^2) \right] (C_{12}^W + C_{23}^W) \\ &\quad + 4(1 - 4c_W^2) C_0^W, \\ F_{\gamma,W} &= 4 \left( \frac{M_H^2}{M_W^2} + 6 \right) (C_{12}^W + C_{23}^W) + 16C_0^W, \\ F_t &= C_0^t + 4C_{12}^t + 4C_{23}^t \end{aligned} \quad (12)$$

where the three-point functions  $C_{ij}^t$  and  $C_{ij}^W$  are defined as

$$\begin{aligned} C_{ij}^t &= C_{ij}^t(s, 0, M_H^2; M_t^2, M_t^2, M_t^2), \\ C_{ij}^W &= C_{ij}^W(s, 0, M_H^2; M_W^2, M_W^2, M_W^2), \end{aligned} \quad (13)$$

and  $C_0$  is the Passarino–Veltman scalar function [29].

We first calculate the SM loop corrections in FormCalc [30] and LoopTools [31]. Our analytical and numerical results are consistent with those in Refs. [19]. We then incorporate the HZ $\gamma$  and H $\gamma\gamma$  anomalous couplings in our calculation to examine their respective impacts on the H $\gamma$  production.

In order to quantify the NP effects, we separate the total cross section of the H $\gamma$  production ( $\sigma_t$ ) into the following three pieces:

$$\begin{aligned} \sigma_t &= \sigma_{\text{SM}} + \left[ \sigma_{\text{IN}}^{(1)} \mathcal{F}_{Z\gamma} + \sigma_{\text{IN}}^{(2)} \mathcal{F}_{\gamma\gamma} \right] \left( \frac{2 \text{ TeV}}{\Lambda} \right)^2 \\ &\quad + \left[ \sigma_{\text{NP}}^{(1)} \mathcal{F}_{Z\gamma}^2 + \sigma_{\text{NP}}^{(2)} \mathcal{F}_{\gamma\gamma}^2 + \sigma_{\text{NP}}^{(3)} \mathcal{F}_{Z\gamma} \mathcal{F}_{\gamma\gamma} \right] \left( \frac{2 \text{ TeV}}{\Lambda} \right)^4, \end{aligned} \quad (14)$$

where  $\sigma_{\text{SM}}$  is the cross section in the SM,  $\sigma_{\text{IN}}^{(1,2)}$  is the interference effect between the SM and NP contributions and  $\sigma_{\text{NP}}^{(1,2,3)}$  is the NP contribution. Figs. 2(a), (d) and (g) show each individual contribution above as a function of  $\sqrt{s}$  for  $m_H = 125$  GeV. The SM contribution falls with  $\sqrt{s}$  and decreases rapidly around the top-quark pair threshold of  $\sqrt{s} \sim 350$  GeV. The fall-off is owing to the cancellation between the  $W$ -boson loop and  $t$ -quark loop contributions. When  $\sqrt{s} \simeq 2m_t$ , the virtual top-quark loop develops an imaginary part and thus contributes maximally. Above the top-quark pair threshold, the cross section drops smoothly with  $\sqrt{s}$  as expected. The interference effect ( $\sigma_{\text{IN}}^{(1,2)}$ ) exhibits a similar behavior to the SM contribution and drops with  $\sqrt{s}$ . On the other hand, the NP contributions ( $\sigma_{\text{NP}}^{(1,2)}$ ) increase with  $\sqrt{s}$  as they are induced by a high-dimensional operator.

The interference effects between the SM and NP depend on the sign of the effective HZ $\gamma$  and H $\gamma\gamma$  couplings. We plot in Fig. 2(b) the total cross section for  $\mathcal{F}_{Z\gamma} = \pm 1$ . For reference,  $\sigma_{\text{SM}}$ , i.e.  $\mathcal{F}_{Z\gamma} = 0$ , is also plotted. For a large  $\mathcal{F}_{Z\gamma}$ , the NP contribution dominates over the interference and SM contributions. We also plot in Fig. 2(c) the total cross section for  $\mathcal{F}_{Z\gamma} = \pm 0.1$  to illustrate the interference effects. For a small  $\mathcal{F}_{Z\gamma}$ , we can ignore the NP contribution, as it is proportional to  $\mathcal{F}_{Z\gamma}^2$ . Therefore, the interference effects yield three similar curves. This discussion above is also applied to  $\mathcal{F}_{\gamma\gamma}$  displayed in Figs. 2(d), (e), (f).

For illustration we list the total cross section (in units of femtobarns) for four benchmark c.m. energies ( $\sqrt{s}$ ) as follows:

$$\begin{aligned} 250 \text{ GeV}: \sigma_t &= 0.1004 + [0.3109 \mathcal{F}_{Z\gamma} + 0.3465 \mathcal{F}_{\gamma\gamma}] \left( \frac{2 \text{ TeV}}{\Lambda} \right)^2 + [0.3828 \mathcal{F}_{Z\gamma}^2 + 0.7872 \mathcal{F}_{\gamma\gamma}^2 + 0.1195 \mathcal{F}_{Z\gamma} \mathcal{F}_{\gamma\gamma}] \left( \frac{2 \text{ TeV}}{\Lambda} \right)^4; \\ 350 \text{ GeV}: \sigma_t &= 0.0341 + [0.2524 \mathcal{F}_{Z\gamma} + 0.0105 \mathcal{F}_{\gamma\gamma}] \left( \frac{2 \text{ TeV}}{\Lambda} \right)^2 + [0.5212 \mathcal{F}_{Z\gamma}^2 + 1.2392 \mathcal{F}_{\gamma\gamma}^2 + 0.1750 \mathcal{F}_{Z\gamma} \mathcal{F}_{\gamma\gamma}] \left( \frac{2 \text{ TeV}}{\Lambda} \right)^4; \end{aligned}$$

$$\begin{aligned}
 500 \text{ GeV: } \sigma_t &= 0.0524 + [0.2865\mathcal{F}_{Z\gamma} + 0.3613\mathcal{F}_{\gamma\gamma}] \left(\frac{2 \text{ TeV}}{\Lambda}\right)^2 + [0.6012\mathcal{F}_{Z\gamma}^2 + 1.5375\mathcal{F}_{\gamma\gamma}^2 + 0.2093\mathcal{F}_{Z\gamma}\mathcal{F}_{\gamma\gamma}] \left(\frac{2 \text{ TeV}}{\Lambda}\right)^4; \\
 1000 \text{ GeV: } \sigma_t &= 0.0214 + [0.1703\mathcal{F}_{Z\gamma} + 0.2808\mathcal{F}_{\gamma\gamma}] \left(\frac{2 \text{ TeV}}{\Lambda}\right)^2 + [0.6614\mathcal{F}_{Z\gamma}^2 + 1.7799\mathcal{F}_{\gamma\gamma}^2 + 0.2362\mathcal{F}_{Z\gamma}\mathcal{F}_{\gamma\gamma}] \left(\frac{2 \text{ TeV}}{\Lambda}\right)^4;
 \end{aligned} \tag{15}$$

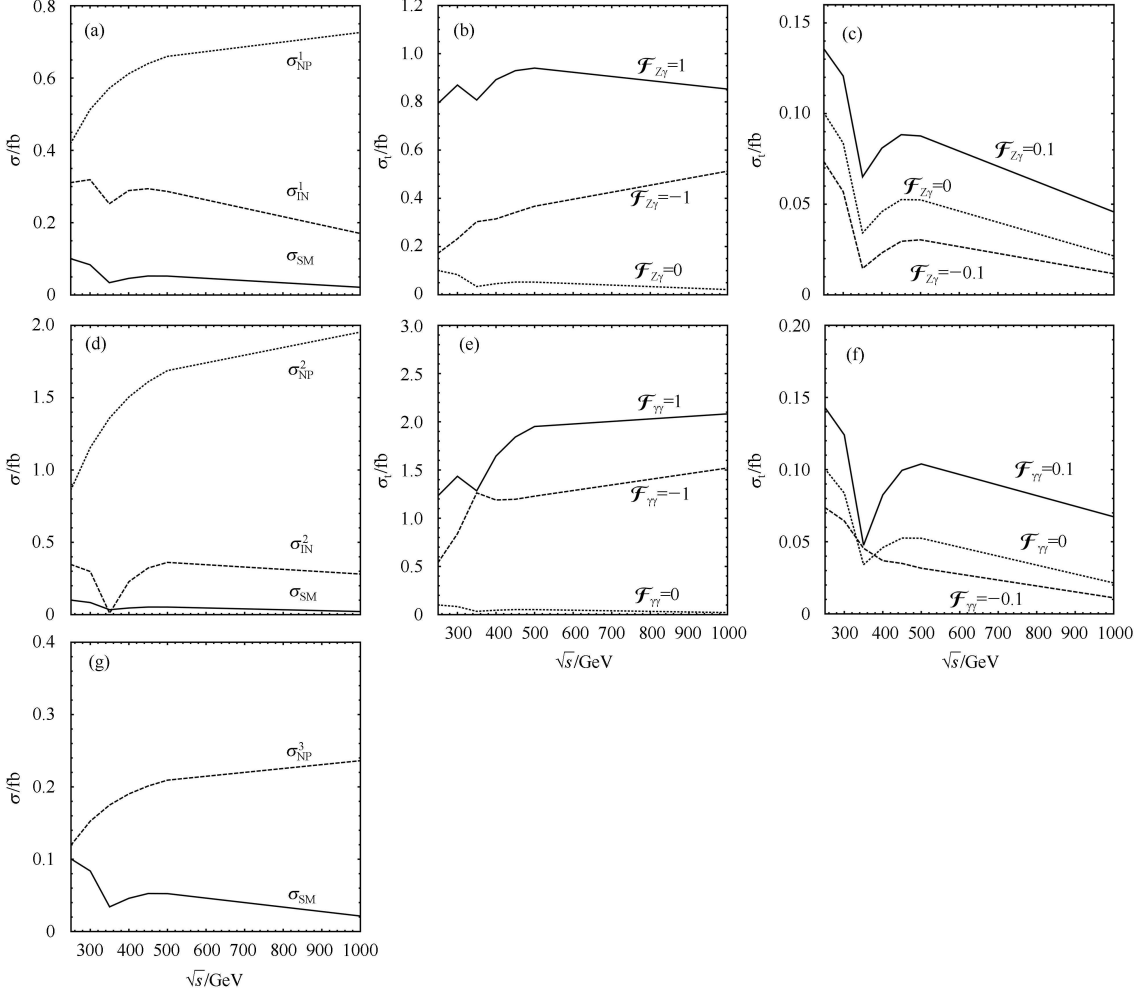


Fig. 2. The cross section of  $e^+e^- \rightarrow H\gamma$  as a function of  $\sqrt{s}$ : (a), (d) and (g) show each individual contribution of  $\sigma_{\text{SM}}$  (solid),  $\sigma_{\text{IN}}^{(1,2)}$  (dashed) and  $\sigma_{\text{NP}}^{(1,2,3)}$  (dotted); (b) and (e) show the total cross section for  $\Lambda=2 \text{ TeV}$  and  $\mathcal{F}_{Z\gamma/\gamma\gamma}=0, \pm 1$ ; (c) and (f) show the total cross section for  $\Lambda=2 \text{ TeV}$  and  $\mathcal{F}_{Z\gamma/\gamma\gamma}=0, \pm 0.1$ .

### 3 Collider simulation and discussion

In this section, we discuss how to detect the  $HZ\gamma$  and  $H\gamma\gamma$  anomalous couplings at the  $e^+e^-$  collider with various c.m. energies. First we focus on the contribution of  $HZ\gamma$  with the  $b\bar{b}$  mode of the Higgs boson decay where  $\mathcal{F}_{Z\gamma}=1$  and  $\mathcal{F}_{\gamma\gamma}=0$ . The collider signature of interest to us is one hard photon and two b-jets. We generate the dominant backgrounds with MadGraph [32]

$$e^+ + e^- \rightarrow \gamma + \gamma^*/Z^* \rightarrow \gamma + b + \bar{b}. \tag{16}$$

At the analysis level, all signal and background events are required to pass the following selection cuts:

$$\begin{aligned}
 p_T^\gamma &> 25 \text{ GeV}, & p_T^b &\geq 25 \text{ GeV}, & p_T^{\bar{b}} &\geq 25 \text{ GeV}, \\
 |\eta^\gamma| &\leq 3.5, & |\eta^b| &\leq 3.5, & |\eta^{\bar{b}}| &\leq 3.5, \\
 \Delta R_{b\bar{b}} &\geq 0.7, & \Delta R_{b\gamma} &\geq 0.7, & \Delta R_{\bar{b}\gamma} &\geq 0.7,
 \end{aligned} \tag{17}$$

where  $p_T^i$  and  $\eta^i$  denote the transverse momentum and pseudo-rapidity of particle  $i$ , respectively. The separation  $\Delta R$  in the azimuthal angle-pseudo-rapidity ( $\phi$ - $\eta$ )

plane between objects  $k$  and  $l$  is

$$\Delta R_{kl} \equiv \sqrt{(\eta_k - \eta_l)^2 + (\phi_k - \phi_l)^2}. \quad (18)$$

For simplicity we ignore the effects due to the finite resolution of the detector. As shown in the CEPC Pre-CDR [25] and ILC CDR [33], the tagging efficiency is 90% for b-quarks and about 10% of charm quarks can be misidentified as a b-quark. The fake-charm background is produced in the following process

$$e^+ + e^- \rightarrow \gamma + \gamma^* / Z^* \rightarrow \gamma + c + \bar{c}, \quad (19)$$

whose contribution is about 1% of the total background when the two b-quarks are tagged. On the other hand, both the signal and  $b\bar{b}$  background are reduced by a factor of 0.8.

Figure 3 plots the  $p_T$  distribution of the photon and b-jets for  $\sqrt{s} = 250$  GeV and 500 GeV. The photon in the signal event exhibits a hard transverse momentum to balance the motion of the Higgs boson. On the other hand, the photon in the SM background is mainly radiated out from the initial state electron and peaks at small  $p_T$  owing to collinear enhancement; see Figs. 3(a) and (c). The anomalous HZ $\gamma$  coupling yields a more en-

ergetic photon in the final state and the effects tend to be more evident with increasing  $\sqrt{s}$ ; see Fig. 3(c). Since the b-jets in the signal are from the Higgs boson decay while those in the background are mainly from a Z-boson decay, the signal exhibits a hard  $p_T$  distribution of the b-jet; see Figs. 3(b) and (d). Similar conclusions also apply to other values of  $\mathcal{F}_{Z\gamma/\gamma\gamma}$ .

To compare the relevant background event rates ( $\mathcal{B}$ ) to the signal event rates ( $\mathcal{S}$ ), we assume an integrated luminosity of  $1 \text{ ab}^{-1}$ . The numbers of signal and background events after imposing the above selection cuts are summarized in the second, fourth, eighth and twelfth rows of Table 1. We consider three kinds of signal: one is induced solely by the SM loop corrections, the other two are generated both by the SM loop correction and by NP effects where  $\mathcal{F}_{Z\gamma} = 1, \mathcal{F}_{\gamma\gamma} = 0$  for one and  $\mathcal{F}_{Z\gamma} = 0, \mathcal{F}_{\gamma\gamma} = 1$  for the other. The former is named the  $\mathcal{S}_{\text{SM}}$ , shown in the fourth to sixth rows in Table 1, while the latter are denoted as the  $\mathcal{S}_{Z\gamma/\gamma\gamma}$ , shown in the seventh to fourteenth rows. Obviously, the backgrounds are larger than the signals by three or four orders of magnitude. One has to impose other cuts to extract the small signal out of the huge background.

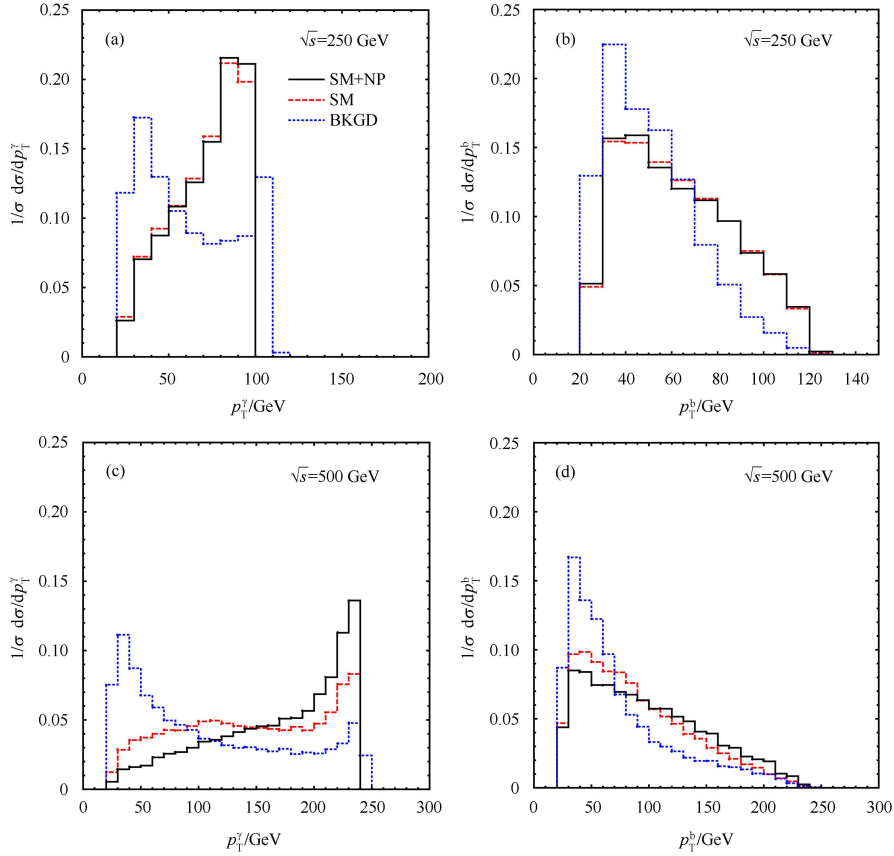


Fig. 3. (color online) The normalized distributions of  $p_T^\gamma$  and  $p_T^b$  of the signal (red and black curve) and background (blue curve) for  $\sqrt{s} = 250$  GeV and 500 GeV. The black curve shows the contribution of the SM and NP operator while the red curve shows the SM contribution alone.

In the signal the photon is produced in association with the Higgs boson. As a result, the energy of the photon is fixed for a given c.m. energy

$$E_\gamma = \frac{s - m_H^2}{2\sqrt{s}}. \quad (20)$$

One can trigger the Higgs boson event from the recoil mass against the photon, defined as  $M_R$ . Fig. 4 displays the recoil mass distribution of the signal events (red-peak) and the background events (blue) for  $\sqrt{s} = 250$  GeV. The background events exhibit a continuous distribution with a peak around  $m_Z$ . It also has a long tail in the region around  $m_H$  owing to the Z-boson width. The difference in the recoil mass distribution between the signal and background events remains at other  $\sqrt{s}$  of the  $e^+e^-$  collider. We impose a hard cut on  $M_R$  to suppress the background. Following Ref. [34] we demand that the recoil mass  $M_R$  lies within a mass window of 5 GeV around  $m_H$ , i.e.

$$\Delta M_R \equiv |M_R - m_H| \leq 5 \text{ GeV}. \quad (21)$$

The  $\Delta M_R$  cut suppresses the background dramatically; for example, for almost all the c.m. energies, less than 1% of the background survives after the  $\Delta M_R$  cut. On the other hand, most of the signal events pass the recoil mass window cut. Unfortunately, the SM contribution alone still cannot be observed owing to the tiny production rate; see the fifth row in Table 1. For  $\mathcal{F}_{Z\gamma} = 1$ ,  $\mathcal{F}_{\gamma\gamma} = 0$  and  $\mathcal{F}_{Z\gamma} = 0$ ,  $\mathcal{F}_{\gamma\gamma} = 1$ , both the anomalous  $HZ\gamma$  coupling and  $H\gamma\gamma$  coupling lead to a few hundreds of signal events each after the recoil mass window cut and thus are testable experimentally. The significance ( $\mathcal{S}_{Z\gamma/\gamma\gamma}/\sqrt{\mathcal{B}}$ ) increases with  $\sqrt{s}$  owing both to the non-renormalizable feature of the high-dimensional operators and to the decreasing SM backgrounds.

Table 1. The number of events of the signal ( $\mathcal{S}_{SM/Z\gamma/\gamma\gamma}$ ) and the background ( $\mathcal{B}$ ) for various c.m. energies ( $\sqrt{s}$ ). The signal is further divided into the SM contribution only ( $\mathcal{S}_{SM}$ ) and the contribution of both the SM and NP effects ( $\mathcal{S}_{Z\gamma/\gamma\gamma}$ ). For illustration we choose  $\Lambda = 2$  TeV,  $\mathcal{F}_{Z\gamma} = 1$ ,  $\mathcal{F}_{\gamma\gamma} = 0$  for  $\mathcal{S}_{Z\gamma}$  and  $\mathcal{F}_{Z\gamma} = 0$ ,  $\mathcal{F}_{\gamma\gamma} = 1$  for  $\mathcal{S}_{\gamma\gamma}$ . The integrated luminosity is chosen to be  $1 \text{ ab}^{-1}$ .

$\sqrt{s}$ (GeV)		250	350	500	1000
$\mathcal{B}$	selection cuts ( $\times 10^5$ )	5.735	3.383	1.960	0.566
	$\Delta M_R$ cut	6112	3194	1683	380
$\mathcal{S}_{SM}$ $ee \rightarrow H\gamma, H \rightarrow b\bar{b}$	selection cuts	58	21	33	12
	$\Delta M_R$ cut	46	17	26	10
$\mathcal{S}_{SM}/\sqrt{\mathcal{B}}$		0.598	0.297	0.648	0.495
$\mathcal{S}_{Z\gamma}$ ( $ee \rightarrow H\gamma$ )		635	646	752	682
$\mathcal{S}_{Z\gamma}$ $ee \rightarrow H\gamma, H \rightarrow b\bar{b}$	selection cuts	361	386	455	273
	$\Delta M_R$ cut	361	386	455	273
$\mathcal{S}_{Z\gamma}/\sqrt{\mathcal{B}}$		4.68	6.84	11.16	14.04
$\mathcal{S}_{\gamma\gamma}$ ( $ee \rightarrow H\gamma$ )		987	1027	1561	1666
$\mathcal{S}_{\gamma\gamma}$ $ee \rightarrow H\gamma, H \rightarrow b\bar{b}$	selection cuts	561	603	944	667
	$\Delta M_R$ cut	561	603	944	667
$\mathcal{S}_{\gamma\gamma}/\sqrt{\mathcal{B}}$		7.2	10.7	23.7	34.4

We now use the results of the last section to discuss the potential of testing the  $HZ\gamma$ ,  $H\gamma\gamma$  couplings at the electron-positron linear collider. Most attention is paid to the scenario in which only one of the  $HZ\gamma$  and  $H\gamma\gamma$  anomalous couplings is nonzero. We first consider the discovery of  $HZ\gamma$  and  $H\gamma\gamma$  anomalous couplings at the electron-positron linear collider. Demanding  $5\sigma$  significance,  $\mathcal{S}_{Z\gamma/\gamma\gamma} = 5\sqrt{\mathcal{B}}$ , yields the discovery potential of the  $HZ\gamma/H\gamma\gamma$  coupling in the scattering of  $e^+e^- \rightarrow H\gamma$ . Figs. 5(a), (d) display the  $5\sigma$  significance curve (dashed line). The shaded regions are good for the discovery of

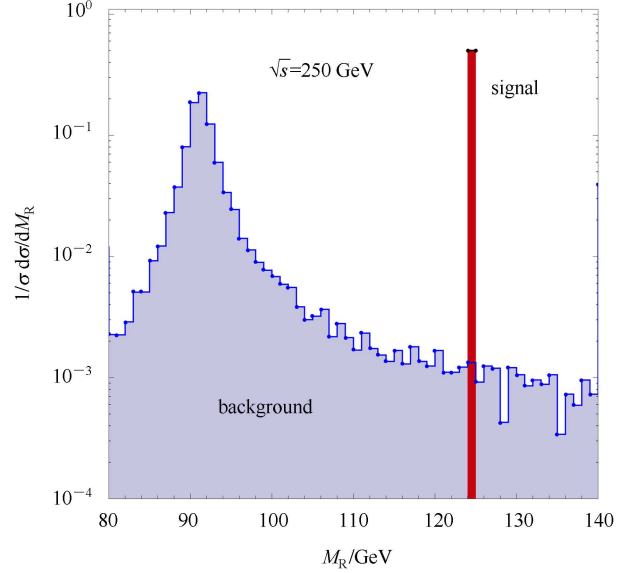


Fig. 4. (color online) The normalized  $M_R$  distributions of the signal and background for  $\sqrt{s} = 250$  GeV.

the anomalous  $\text{HZ}\gamma/\text{H}\gamma\gamma$  coupling. Owing to the SM contribution and the interference effects, the discovery regions are asymmetric around  $\mathcal{F}_{\text{Z}\gamma/\gamma\gamma}=0$ . We also plot the CMS exclusion limits of the  $\text{HZ}\gamma/\text{H}\gamma\gamma$  coupling. We note that the discovery potential of  $\text{HZ}\gamma$  coupling at the  $e^-e^+$  collider at  $\sqrt{s}=250$  GeV is marginally close to the current CMS exclusion limit. With the c.m. energy increased from 250 GeV to 1000 GeV, the  $e^+e^-$  collider could cover the regions of  $0.50 < \mathcal{F}_{\text{Z}\gamma} < 1.03$  and  $-2.02 < \mathcal{F}_{\text{Z}\gamma} < -0.76$ , which cannot be probed at the 8 TeV LHC; while the discovery potential of the  $\text{H}\gamma\gamma$  coupling could cover the non-exclusion red region of  $\mathcal{F}_{\gamma\gamma}\sim 0.56$  at an  $e^-e^+$  collider with  $\sqrt{s}\geq 400$  GeV.

The CMS limits are derived from the Higgs boson decay as follows. The partial decay widths of  $\text{H}\rightarrow\text{Z}\gamma$  and  $\text{H}\rightarrow\gamma\gamma$  are given by

$$\Gamma(\text{H}\rightarrow\text{Z}\gamma) = \frac{m_{\text{H}}^3}{8\pi v^2} \left(1 - \frac{m_{\text{Z}}^2}{m_{\text{H}}^2}\right)^3 \left| \mathcal{F}_{\text{Z}\gamma}^{\text{SM}} + \frac{v^2}{\Lambda^2} \mathcal{F}_{\text{Z}\gamma} \right|^2, \quad (22)$$

$$\Gamma(\text{H}\rightarrow\gamma\gamma) = \frac{m_{\text{H}}^3}{16\pi v^2} \left| \mathcal{F}_{\gamma\gamma}^{\text{SM}} + \frac{v^2}{\Lambda^2} \mathcal{F}_{\gamma\gamma} \right|^2, \quad (23)$$

where  $\mathcal{F}_{\text{Z}\gamma}^{\text{SM}}, \mathcal{F}_{\gamma\gamma}^{\text{SM}}$ , induced by the W boson and fermion loops in the SM, are given by [5, 35]

$$\mathcal{F}_{\text{Z}\gamma}^{\text{SM}} = \frac{\alpha}{4\pi s_{\text{W}} c_{\text{W}}} \left( 3 \frac{Q_{\text{t}}(2T_3^{\text{t}} - 4Q_{\text{t}} s_{\text{W}}^2)}{c_{\text{W}}} A_{1/2}^{\text{H}}(\tau_{\text{t}}, \lambda_{\text{t}}) + c_{\text{W}} A_1^{\text{H}}(\tau_{\text{W}}, \lambda_{\text{W}}) \right), \quad (24)$$

$$\mathcal{F}_{\gamma\gamma}^{\text{SM}} = \frac{\alpha}{4\pi} \left( 3Q_{\text{t}}^2 A_{1/2}^{\text{H}}(\tau_{\text{t}}^{-1}) + A_1^{\text{H}}(\tau_{\text{W}}^{-1}) \right). \quad (25)$$

The functions,  $A_{1/2}^{\text{H}}(\tau_i, \lambda_i)$ ,  $A_1^{\text{H}}(\tau_i, \lambda_i)$ ,  $A_{1/2}^{\text{H}}(\tau_i)$  and  $A_1^{\text{H}}(\tau_i)$ , are given in Ref. [36] where  $\tau_i = 4m_i^2/m_{\text{H}}^2$  and  $\lambda_i = 4m_i^2/m_{\text{Z}}^2$ .  $Q_{\text{t}}$  is the top-quark electric charge in units of  $|e|$  and  $T_3^{\text{t}} = 1/2$ . In the SM  $\mathcal{F}_{\text{Z}\gamma}^{\text{SM}} \sim 0.007$ ,  $\mathcal{F}_{\gamma\gamma}^{\text{SM}} \sim -0.004$  for  $m_{\text{H}} = 125$  GeV [37]. The CMS measurement requires

$$\frac{\Gamma(\text{H}\rightarrow\text{Z}\gamma)}{\Gamma_{\text{SM}}(\text{H}\rightarrow\text{Z}\gamma)} \leq 9.5,$$

$$0.91 \leq \frac{\Gamma(\text{H}\rightarrow\gamma\gamma)}{\Gamma_{\text{SM}}(\text{H}\rightarrow\gamma\gamma)} \leq 1.4, \quad (26)$$

which yields the CMS exclusion bounds shown in

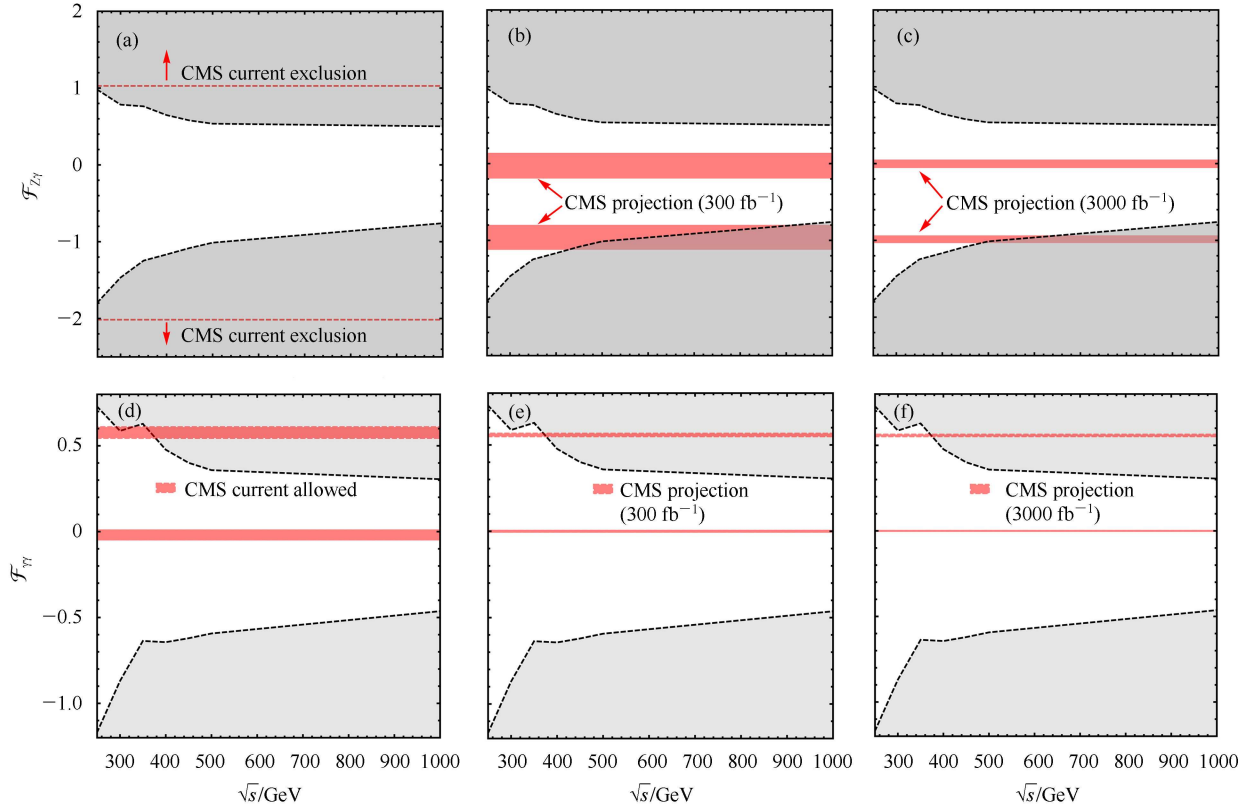


Fig. 5. (color online) Discovery potential of the  $\text{HZ}\gamma/\text{H}\gamma\gamma$  anomalous coupling at the  $e^+e^-$  collider as a function of  $\sqrt{s}$  for  $\mathcal{L}=1000$   $\text{fb}^{-1}$  and  $\Lambda=2$  TeV. The shaded regions above or below the black-dashed curves are good for discovery. The CMS exclusion limits and allowed regions obtained from the Higgs boson rare decay are also shown for comparison (see the horizontal red-dashed curves and red regions): (a) CMS exclusion limits ( $\sqrt{s}=8$  TeV and  $\mathcal{L}=19$   $\text{fb}^{-1}$ ); (d) CMS allowed regions ( $\sqrt{s}=8$  TeV and  $\mathcal{L}=19$   $\text{fb}^{-1}$ ); (b), (e) CMS projection allowed regions ( $\sqrt{s}=14$  TeV and  $\mathcal{L}=300$   $\text{fb}^{-1}$ ); (c), (f) CMS projection allowed regions ( $\sqrt{s}=14$  TeV and  $\mathcal{L}=3000$   $\text{fb}^{-1}$ ).

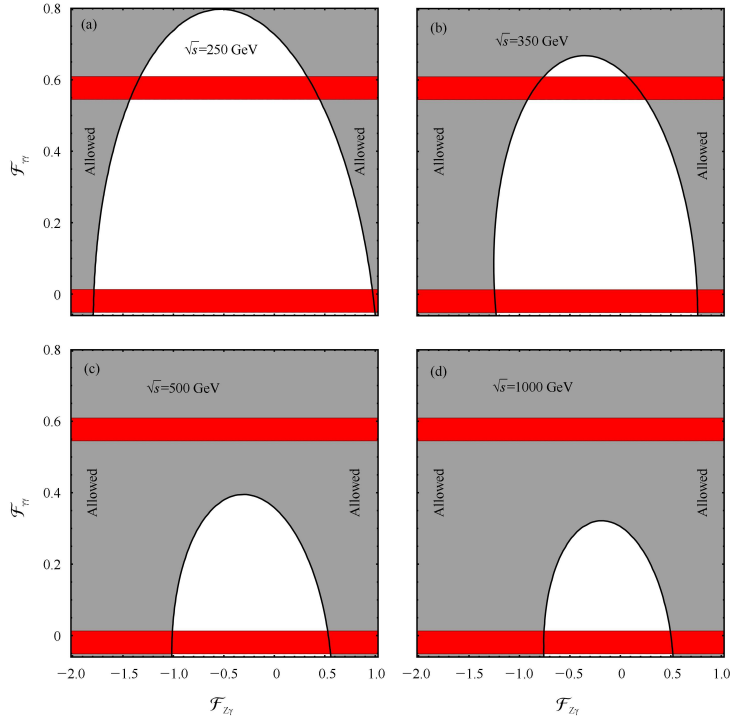


Fig. 6. (color online) The total cross section of  $H\gamma$  production at an  $e^-e^+$  collider changes as a function of  $\mathcal{F}_{Z\gamma}$  and  $\mathcal{F}_{\gamma\gamma}$ . The red regions are non-exclusive according to the current CMS data and the red regions outside the black lines show the discovery potential of the  $e^-e^+$  collider.

Figs. 5(a) and (d), one bound on  $\mathcal{F}_{Z\gamma}$  as  $-2.02 \leq \mathcal{F}_{Z\gamma} \leq 1.03$ , two bounds on  $\mathcal{F}_{\gamma\gamma}$  as  $-0.051 \leq \mathcal{F}_{\gamma\gamma} \leq 0.013$  and  $0.55 \leq \mathcal{F}_{\gamma\gamma} \leq 0.62$ ; see the horizontal black-dashed curves and red regions.

A recent study on projected performance of an upgraded CMS detector at the LHC and high luminosity LHC (HL-LHC) [38] shows that the  $H \rightarrow Z\gamma$  process is expected to be measured at the 14 TeV LHC with  $\sim 60\%$  and  $\sim 20\%$  uncertainties at the 95% confidence level using an integrated dataset of  $300 \text{ fb}^{-1}$  and  $3000 \text{ fb}^{-1}$ , respectively, while for the  $H \rightarrow \gamma\gamma$  process, the uncertainties are  $\sim 6\%$  and  $\sim 4\%$ . We plot the corresponding CMS projection limits in Figs. 5(b), (e) and Figs. 5(c), (f). Future experiments at the LHC and HL-LHC are expected to impose tighter bounds on  $\mathcal{F}_{Z\gamma/\gamma\gamma}$ . When  $\sqrt{s} \geq 500 \text{ GeV}$ , an  $e^+e^-$  collider has a better performance in probing the negative  $\mathcal{F}_{Z\gamma}$  than the LHC and HL-LHC. For  $\mathcal{F}_{\gamma\gamma} \sim 0.56$ , an  $e^+e^-$  collider with  $\sqrt{s} \geq 400 \text{ GeV}$  has a better discovery potential than the LHC and HL-LHC; see the overlapping regions of the red region and shaded region.

When both the  $HZ\gamma$  and  $H\gamma\gamma$  couplings are considered, Fig. 6 displays the total cross section of  $H\gamma$  production changing as a function of  $\mathcal{F}_{Z\gamma}$  and  $\mathcal{F}_{\gamma\gamma}$  with various energies. The allowed discovery regions of  $\mathcal{F}_{Z\gamma}$  and  $\mathcal{F}_{\gamma\gamma}$  are the red regions outside the black lines. With the c.m. energy increased from 250 GeV to 1000 GeV, more and

more red regions can be discovered. When  $\sqrt{s} \geq 500 \text{ GeV}$ , the non-exclusive red region of  $\mathcal{F}_{\gamma\gamma} \sim 0.56$  is entirely allowed. For more detail, see Eqs. (15).

## 4 Further analysis

The  $HZ\gamma$  and  $H\gamma\gamma$  anomalous couplings affect both the Higgs boson decay and  $H\gamma$  production, but their interference effects with the SM contributions is different for the two processes. In order to examine the different interference effects, we define a ratio of the cross section of the  $H\gamma$  production,  $R_\sigma$ , a ratio of the width of  $H \rightarrow Z\gamma/\gamma\gamma$  decay,  $R_{Z\gamma/\gamma\gamma}$ , and the relative sign  $\mu_{Z\gamma/\gamma\gamma}$ , as follows:

$$\begin{aligned}
 R_\sigma &\equiv \frac{\sigma_t(e^+e^- \rightarrow H\gamma)}{\sigma_{\text{SM}}(e^+e^- \rightarrow H\gamma)}, \\
 R_{Z\gamma} &\equiv \frac{\Gamma(H \rightarrow Z\gamma)}{\Gamma_{\text{SM}}(H \rightarrow Z\gamma)}, & \mu_{Z\gamma} &= \text{sign}\left(\frac{\mathcal{F}_{Z\gamma}}{\mathcal{F}_{Z\gamma}^{\text{SM}}}\right), \\
 R_{\gamma\gamma} &\equiv \frac{\Gamma(H \rightarrow \gamma\gamma)}{\Gamma_{\text{SM}}(H \rightarrow \gamma\gamma)}, & \mu_{\gamma\gamma} &= \text{sign}\left(\frac{\mathcal{F}_{\gamma\gamma}}{\mathcal{F}_{\gamma\gamma}^{\text{SM}}}\right). \quad (27)
 \end{aligned}$$

Figure 7 displays the strong correlation between  $R_\sigma$  and  $R_{Z\gamma/\gamma\gamma}$  for several c.m. energies when one anomalous coupling is considered at a time; see the red-dashed curves. There are two values of  $R_\sigma$  for each fixed  $R_{Z\gamma/\gamma\gamma}$ ; the larger value  $R_\sigma$  corresponds to  $\mu_{Z\gamma/\gamma\gamma} < 0$  while the

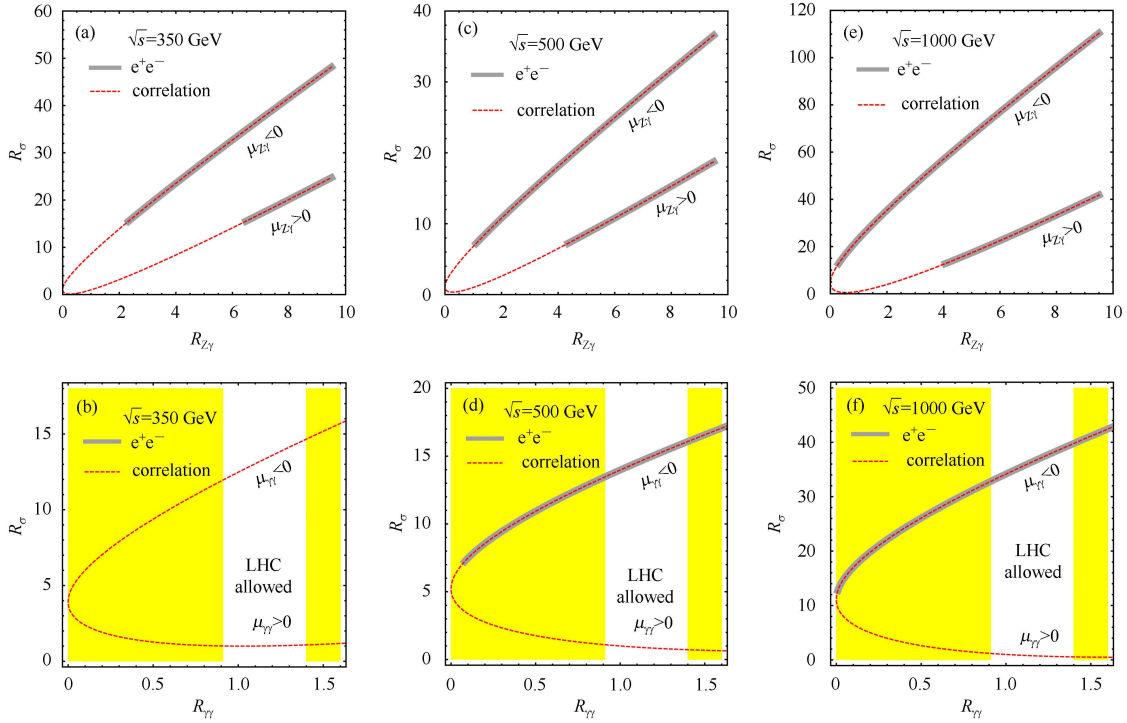


Fig. 7. (color online) Correlations between  $R_\sigma$  and  $R_{ZY/\gamma\gamma}$  (red-dashed line) and discovery region at the  $e^+e^-$  colliders (bold-gray curve). The yellow shaded regions are excluded by recent CMS data.

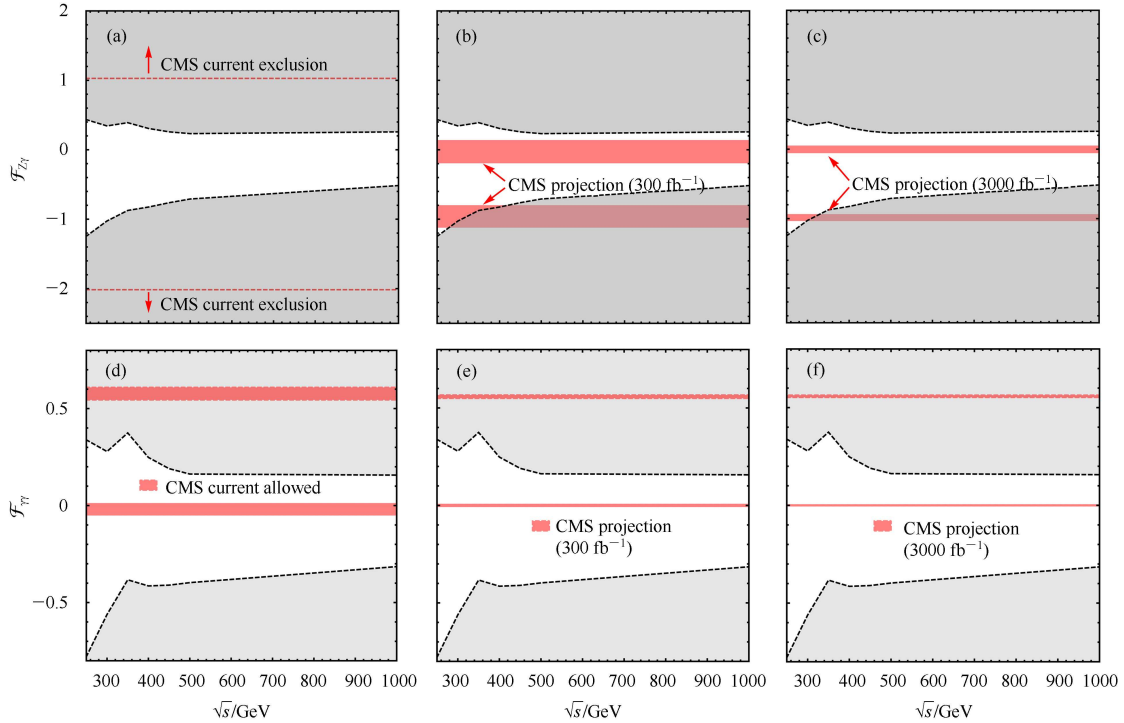


Fig. 8. (color online) Lower bounds and allowed regions of  $\mathcal{F}_{ZY/\gamma\gamma}$  as a function of  $\sqrt{s}$  obtained in Higgs production for  $\mathcal{L}=1000 \text{ fb}^{-1}$  and  $\Lambda=2 \text{ TeV}$ . The shaded regions above or below the black-dashed curves are for exclusion. The CMS exclusion limits obtained from the Higgs boson rare decays are shown for comparison (horizontal red-dashed curves): (a), (d) CMS exclusion limits ( $\sqrt{s}=8 \text{ TeV}$  and  $\mathcal{L}=19 \text{ fb}^{-1}$ ); (b), (e) CMS projection limits ( $\sqrt{s}=14 \text{ TeV}$  and  $\mathcal{L}=300 \text{ fb}^{-1}$ ); (c), (f) CMS projected limits ( $\sqrt{s}=14 \text{ TeV}$  and  $\mathcal{L}=3000 \text{ fb}^{-1}$ ).

smaller value corresponds to  $\mu_{Z\gamma/\gamma\gamma} > 0$ . The two-fold ambiguity in the  $\Gamma(H \rightarrow Z\gamma/\gamma\gamma)$  measurement can be resolved by precise knowledge of  $R_\sigma$  if the  $\mathcal{F}_{Z\gamma/\gamma\gamma}$  is large enough to discover the  $H\gamma$  signal at the  $e^+e^-$  collider. In Fig. 7 we also plot the discovery region of  $R_{Z\gamma/\gamma\gamma}$  in the scattering of  $e^+e^- \rightarrow H\gamma$  for various c.m. energies; see the shaded bands. One can uniquely determine both the magnitude and sign of  $\mathcal{F}_{Z\gamma/\gamma\gamma}$  in those shaded-band regions. The discrimination power of the two-fold  $R_\sigma$  for a fixed  $R_{Z\gamma/\gamma\gamma}$  increases dramatically with the c.m. energy of the  $e^+e^-$  collider; for example, for  $R_{Z\gamma} = 9$ ,  $R_\sigma$  is equal to 8 and 10 at a  $\sqrt{s} = 250$  GeV collider while it is equal to 40 and 110 at a  $\sqrt{s} = 1000$  GeV collider. It is worth mentioning that the partial decay width of  $H \rightarrow Z\gamma$  is exactly the same as the SM prediction when  $v^2/\Lambda^2 \mathcal{F}_{Z\gamma} = -2\mathcal{F}_{Z\gamma}^{\text{SM}}$ . In that case one can still observe the anomalous  $HZ\gamma$  coupling at the  $e^+e^-$  collider when  $\sqrt{s} \gtrsim 500$  GeV. For the  $R_{\gamma\gamma}$ , it is highly limited by the current LHC data and yields two solutions of  $\mathcal{F}_{\gamma\gamma}$ : one is  $v^2/\Lambda^2 \mathcal{F}_{\gamma\gamma} \sim -2\mathcal{F}_{\gamma\gamma}^{\text{SM}}$  which could be detected in the  $H\gamma$  production when  $\sqrt{s} \gtrsim 500$  GeV, the other is  $\mathcal{F}_{\gamma\gamma} \sim 0$ , which cannot be probed.

If no NP effects were observed in the  $H\gamma$  production, one could obtain  $2\sigma$  exclusion limits of  $\mathcal{F}_{Z\gamma/\gamma\gamma}$ , which are displayed in Fig. 8. The CMS current and projected sensitivities are also plotted for comparison; see the red-shaded regions.

## 5 Summary

We study the potential of measuring the  $HZ\gamma$  and  $H\gamma\gamma$  anomalous couplings in the process  $e^-e^+ \rightarrow H\gamma$ . Such a scattering process occurs only at loop level in the SM. After considering the interference of the SM loop effects and the anomalous coupling contributions, we performed a collider simulation of the  $H\gamma$  production with  $H \rightarrow b\bar{b}$ . Even though the SM contribution alone cannot be detected, the anomalous couplings can enhance the production rate sizeably and lead to a discovery at a high energy electron-positron collider with an integrated luminosity of  $1 \text{ ab}^{-1}$ .

When considering one anomalous coupling at a time, our study shows that, for negative  $\mathcal{F}_{Z\gamma}$  or  $\mathcal{F}_{\gamma\gamma} \sim 0.56$ , an  $e^+e^-$  collider has better performance than the current LHC and future HL-LHC. When both couplings contribute simultaneously to the  $H\gamma$  production, more parameter regions are allowed and can be fully explored at a high energy  $e^+e^-$  collider.

We also derive exclusion bounds on the anomalous couplings in the case that no NP effects are observed in  $H\gamma$  production. The current CMS data indicates a two-fold solution of the anomalous coupling. Resolving such an ambiguity is beyond the capability of the upgraded LHC or HL-LHC, but can be discriminated easily at an  $e^+e^-$  collider.

## References

- 1 Aad G et al. (ATLAS collaboration). Phys. Rev. D, 2014, **90**: 112015
- 2 Khachatryan V et al. (CMS collaboration). Eur. Phys. J. C, 2014, **74**: 3076
- 3 Aad G et al. (ATLAS collaboration). Phys. Lett. B, 2014, **732**: 8
- 4 Chatrchyan S et al. (CMS collaboration). Phys. Lett. B, 2013, **726**: 587
- 5 Azatov A, Contino R, Di Iura A, Galloway J. Phys. Rev. D, 2013, **88**: 075019
- 6 Arhrib A, Benbrik R, YUAN T C. Eur. Phys. J. C, 2014, **74**: 2892
- 7 Belanger G, Bizouard V, Chalons G. Phys. Rev. D, 2014, **89**: 095023
- 8 Hagiwara K, Stong M. Z. Phys. C, 1994, **62**: 99
- 9 Gounaris G, Renard F, Vlachos N. Nucl. Phys. B, 1996, **459**: 51
- 10 Hagiwara K, Ishihara S, Kamoshita J, Kniehl B A. Eur. Phys. J. C, 2000, **14**: 457
- 11 CAO Q H, Larios F, Tavares-Velasco G, YUAN C P. Phys. Rev. D, 2006, **74**: 056001
- 12 Hankele V, Klamke G, Zeppenfeld D, Figy T. Phys. Rev. D, 2006, **74**: 095001
- 13 Dutta S, Hagiwara K, Matsumoto Y. Phys. Rev. D, 2008, **78**: 115016
- 14 Rindani S D, Sharma P. Phys. Rev. D, 2009, **79**: 075007
- 15 Rindani S D, Sharma P. Phys. Lett. B, 2010, **693**: 134
- 16 REN H Y. arXiv:1503.08307
- 17 Barroso A, Pulido J, Romao J. Nucl. Phys. B, 1986, **267**: 509
- 18 Abbasabadi A, Bowser-Chao D, Dicus D A, Repko W W. Phys. Rev. D, 1995, **52**: 3919
- 19 Djouadi A, Driesen V, Hollik W, Rosiek J. Nucl. Phys. B, 1997, **491**: 68
- 20 HU S L, LIU N, REN J, WU L. J. Phys. G, 2014, **41**: 125004
- 21 Gainer J S, Keung W Y, Low I, Schwaller P. Phys. Rev. D, 2012, **86**: 033010
- 22 Hagiwara K, Szalapski R, Zeppenfeld D. Phys. Lett. B, 1993, **318**: 155
- 23 Achard P et al. (L3). Phys. Lett. B, 2004, **589**: 89
- 24 Masso E, Sanz V, Phys. Rev. D, 2013, **87**: 033001
- 25 <http://cepc.ihep.ac.cn/preCDR/volume.html>
- 26 Baer H, Barklow T, Fujii K, GAO Y, Hoang A et al. arXiv:1306.6352
- 27 Carena M, Low I, Wagner C E. JHEP 2012, **1208**: 060
- 28 Djouadi A. Phys. Rept., 2008, **459**: 1
- 29 Passarino G, Veltman M. Nucl. Phys. B, 1979, **160**: 151
- 30 Hahn T, Perez-Victoria M. Comput. Phys. Commun., 1999, **118**: 153
- 31 van Oldenborgh G. Comput. Phys. Commun., 1991, **66**: 1
- 32 Alwall J, Frederix R, Frixione S, Hirschi V, Maltoni F et al. JHEP, 2014, **1407**: 079
- 33 Behnke T, Brau J E, Foster B, Fuster J, Harrison M et al. arXiv:1306.6327
- 34 Behnke T, Brau J E, Burrows P N, Fuster J, Peskin M et al. arXiv:1306.6329
- 35 Low I, Lykken J, Shaughnessy G. Phys. Rev. D, 2012, **86**: 093012
- 36 Djouadi A. Phys. Rept, 2008, **457**: 1
- 37 CAO Q H, WANG H R, ZHANG Y. arXiv:1503.05060
- 38 CMS collaboration. arXiv:1307.7135